Check for updates

A solvent-dependent chemosensor for fluorimetric detection of Hg^{2+} and colorimetric detection of Cu^{2+} based on a new diarylethene with a rhodamine B unit†

Heng Zhao, Haichang Ding, Huimin Kang, Congbin Fan, [ID] Gang Liu [ID] *
and Shouzhi Pu*

A novel solvent-dependent chemosensor **1o** based on a diarylethene containing a rhodamine B unit has been designed. It could be used as a dual-functional chemosensor for selective detection of Hg^{2+} and Cu^{2+} by monitoring the changes in the fluorescence and UV-vis spectral in different solvents. A striking fluorescence enhancement at 617 nm was observed in DMSO upon the addition of Hg^{2+}. However, **1o** showed a remarkable absorption band appeared with maximum absorption at 555 nm after the addition of Cu^{2+} in THF. The results of ESI-MS spectra and Job's plot confirmed a 1 : 1 binding stoichiometry between **1o** and the two ions. The limits of detection of Hg^{2+} and Cu^{2+} were determined to be 0.14 μM and 0.51 μM, respectively. A 1 : 2 demultiplexer circuit was constructed by using UV light as data input, Cu^{2+} as the address input, and the absorbance at 555 nm and the absorbance ratio of (A_{603}/A_{274}) as the dual data outputs.

Introduction

In recent decades chemosensors for selective detection of a wide variety of metal ions have attracted increasing attention due to their potential practical advantages in analytical, biomedical, and environmental chemistry.[1,2] Among metal ions, Hg^{2+} is considered to be one of the most dangerous and toxic pollutants in the environment and biosphere even in low concentration, because its strong affinity to thiol groups present in proteins and enzymes, can causes the dysfunction of most proteins and enzymes.[3–5] Moreover, Hg^{2+} can be accumulated in the body, and easily penetrate through biological membranes, such as skin, gastrointestinal and respiratory tissues,[6] causing various types of diseases like central nervous system defects, arrhythmia, kidney damage, minamata disease, and cardiomyopathy.[7] On the other hand, the third most abundant essential heavy metal ion (after iron and zinc) present in the human body Cu^{2+} plays a critical role in the physiology of living organisms, its deficiency can lead to a wide range of diseases including anemia, coronary heart disease, hypopigmentation, brain dysfunction and various neurological diseases.[8–11] However, an excessive intake of Cu^{2+} will disturb the cellular homeostasis and lead to many serious neurodegenerative diseases, such as

Alzheimer's disease, Wilson's disease, Parkinson's diseases, and prion diseases.[12–15] Thus, the development of sensitive and selective imaging tools for effective and convenient detection of Hg^{2+} and Cu^{2+} is of great significance for biochemistry and environmental science.

In recent years, diarylethenes have been widely nominated as one of the most attractive photochromic molecules, when they are stimulated by photo irradiation can undergo a reversible transition between open-ring and closed-ring forms with significant changes of absorption/emission spectrum, it is possible to introduce a recognizing group into the diarylethene structure to achieve a fluorescence switch.[16–21] Some of diarylethene-based chemosensors for the detection of a wide species of ions have already been reported.[22–24] For example, Fu *et al.* reported a fluorescence chemosensor for detecting Zn^{2+} based on a new diarylethene with a benzyl-linked 8-aminoquinoline-2-aminomethylpyridine unit.[25] Rhodamine and its derivatives have gained tremendous interest in the field of biosensors because of their advantages such as broad emission wavelength, high fluorescence quantum yield, and large extinction coefficient.[26–28] Generally speaking, rhodamine derivatives with spirolactam structure are non-fluorescent and colorless. Interestingly, upon binding with protons or metal ions they become strongly fluorescent and produce intense color because of ring-opened structure.[29] Therefore, rhodamine derivatives have been widely applied to design chemosensors for naked-eye detecting metal ions.[30] Recently, we have reported a diarylethene-based fluorescent sensor with a rhodamine

Jiangxi Key Laboratory of Organic Chemistry, Jiangxi Science and Technology Normal University, Nanchang, Jiangxi 330013, PR China. E-mail: liugang0926@163.com; pushouzhi@tsinghua.org.cn; Fax: +86-791-83831996; Tel: +86-791-83831996

group which exhibited excellent fluorescence regulation and ion recognition.[31] Nevertheless, most studies in the field of rhodamine-based sensors have only focused on identifying a single metal ion in a single solvent system, only a few sensors have the ability to identify different metal ions in different solvent systems.[28] Thus, the design and synthesize rhodamine-based sensors that have the ability to identify different metal ions in different solvent systems are still a challenge.

In this work, we developed a novel diarylethene-based chemosensor containing a rhodamine B unit for simultaneous Hg^{2+} and Cu^{2+} detection. The chemosensor **1o** displayed a selective colorimetric response to Cu^{2+} with a naked-eye-detectable color change from colorless to pink in THF, while it also showed a fluorometric response selectively to Hg^{2+} with a fluorescent change of color from dark to orange-red in DMSO. Moreover, **1o** exhibited excellent photochromic performance under alternate irradiation with UV light and visible light, and it had been successfully applied to construct a 1 : 2 demultiplexer circuit. The photochromism of **1o** was presented in Scheme 1.
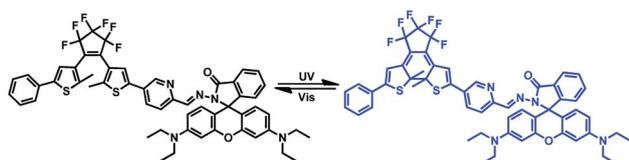
Experimental

General methods

All reagents and solvents were obtained from J&K Scientific Ltd. (Beijing China). NMR spectra of samples were recorded on Bruker AV400 (400 MHz) in DMSO-d_6 or THF-d_8 solution using tetramethylsilane (TMS) as an internal standard. Mass spectrum was recorded on a Bruker Amazon SL Ion Trap Mass Spectrometer under ESI mode. Melting point was measured on a WRS-1B melting point apparatus. The fluorescence quantum yield was obtained with an Edinburgh FLS 1000 fluorescence spectrometer. All the emission spectra were recorded using a Hitachi F-4600 spectrofluorimeter and all the absorption spectra were recorded using an Agilent 8454 UV/vis spectrophotometer.
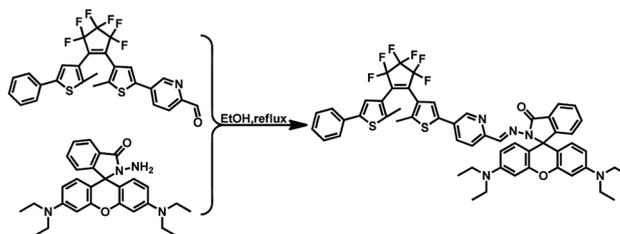
Synthesis

The synthetic protocol of diarylethene (**1o**) was outlined in Scheme 2. Compounds **2** and **3** were readily synthesized in high yields according to literature procedures.[32,33]

Synthesis of 1o. Compound **2** (0.10 g, 0.18 mmol) was added to a stirring solution of rhodamine B hydrazide (0.10 g, 0.21 mmol) in ethanol (5.0 mL). The reaction mixture was stirred and refluxed for 12 h. After the solvent was evaporated under reduced pressure, the crude product was purified by silica gel column chromatography (PE/EtOAc = 2 : 1) to afford pure blue solid of **1o** (0.13 g, 0.13 mmol, 66% yield). Mp: 409–411 K. ^{1}H

Scheme 2 The synthetic pathways of diarylethene **1o**.

NMR (DMSO-d_6, 400 MHz): δ (ppm) 8.81 (s, 1H), 8.41 (s, 1H), 8.10 (d, J = 8.1 Hz, 1H), 8.02 (d, J = 7.4 Hz, 1H), 7.83 (d, J = 8.4 Hz, 1H), 7.76–7.60 (m, 5H), 7.55 (s, 1H), 7.48 (t, J = 7.5 Hz, 2H), 7.41 (d, J = 7.5 Hz, 1H), 7.16 (d, J = 7.5 Hz, 1H), 6.52 (d, J = 12.5 Hz, 4H), 6.40 (d, J = 9.0 Hz, 2H), 3.37 (d, J = 7.3 Hz, 8H), 2.06 (s, 3H), 2.03 (s, 3H), 1.13 (t, J = 6.8 Hz, 12H) (Fig. S1†). ^{13}C NMR (DMSO-d_6, 100 MHz), δ (ppm): 164.67, 153.01, 152.86, 152.32, 149.17, 146.22, 145.14, 143.30, 142.25, 141.72, 138.07, 134.82, 133.69, 132.97, 129.70, 129.30, 128.62, 128.09, 127.90, 125.78, 125.33, 125.02, 124.24, 123.70, 123.02, 119.87, 116.21, 108.69, 105.29, 97.97, 65.65, 44.11, 14.53, 12.89. ESI-MS (m/z): 1010.1 $[M + Na^+]^+$ (Fig. S2†). Anal. calcd for $C_{55}H_{47}F_6N_5O_2S_2$ (%): C, 66.85; H, 4.79; N, 7.09; O, 3.24. Found: C, 66.98; H, 4.78; N, 7.11; O, 3.25.

Results and discussion

Photochromism of 1o

Determination of photochromic properties of **1o** (20 μM) in THF. As shown in Fig. 1, owing to the π–π* transition, its ring-opening form isomer showed an absorption peak at 348 nm.[34] A new absorption band centered at 603 nm appeared along with a color change from colorless to blue upon the irradiation with 297 nm light, which was assigned to the formation of the ring-closed isomer **1c** with π-electron delocalization enhancement through the molecular backbone.[35] Under irradiation using visible light of λ > 500 nm, **1c** blue solution could be bleached to colorless, and its absorption peak 348 nm return to the original

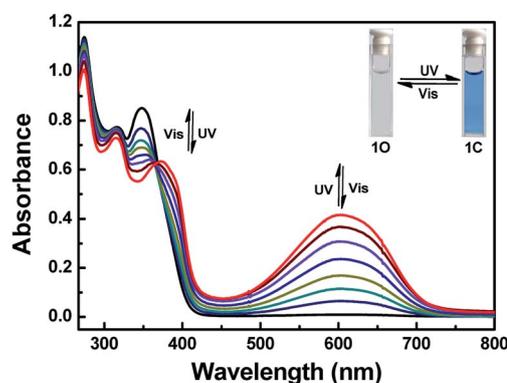Scheme 1 Photochromism of diarylethene **1o**.

Fig. 1 Absorption spectral and color changes of **1o** (20 μM) in THF upon alternating irradiation with UV (λ = 297 nm) and visible lights (λ > 500 nm).
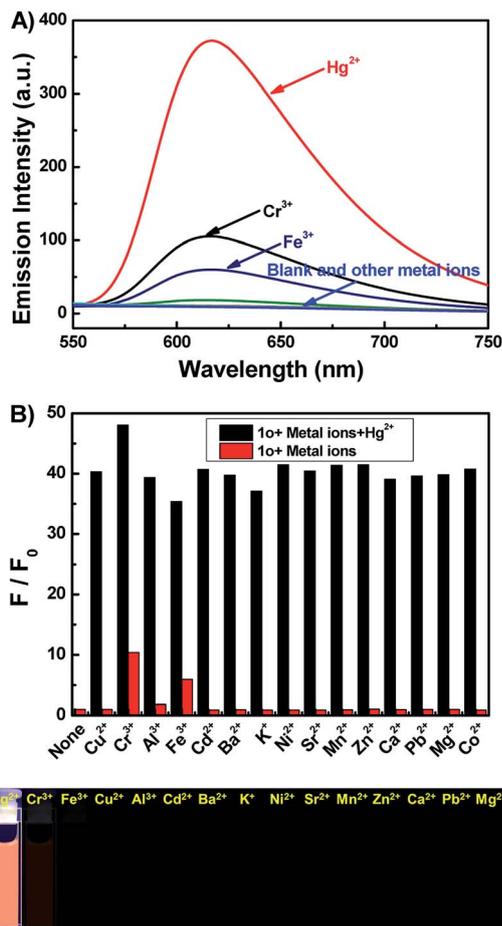
Fig. 2 (A) Fluorescence spectra of **1o** (20 μM) with 10.0 equiv. of different metal ions in DMSO. (B) Effect of competitive metal ions on the interaction between **1o** and Hg^{2+} ion. (C) Photographs of fluorescence.
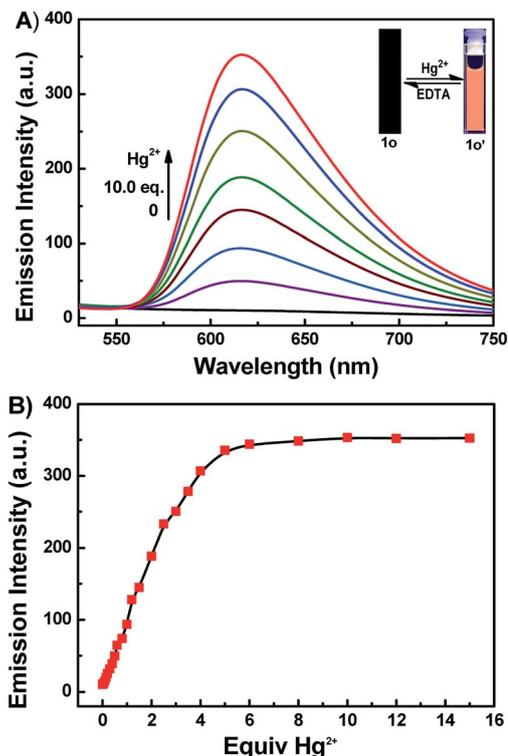

Fig. 3 (A) Fluorescence spectra changes of **1o** in DMSO induced by Hg^{2+}/EDTA. (B) Fluorescence intensity at 617 nm *versus* equivalents of Hg^{2+} added.

state. The isobestic point observed at 366 nm, which suggested a two-component photochromic nature. The quantum yields of the cyclization and cyclization reactions for the determination of **1o** were 0.54 and 0.02, respectively.[36] The fatigue resistance of **1o** indicates that for alternating ultraviolet/visible irradiations, **1o** was only reduced by 10.3% after coloring-discoloration cycles executed ten times (Fig. S3†).

Fluorescent spectra response of 1o to Hg^{2+}

It has been reported that rhodamine B derivatives undergo significant changes in fluorescence spectra when coordinate with metal ions, and thus they can be used as sensitive probes for metal ion detection. The fluorescence spectra of **1o** (20 μM) with 16 metal ions (Cu^{2+}, Hg^{2+}, Cr^{3+}, Fe^{3+}, Ni^{2+}, Zn^{2+}, Ca^{2+}, Pb^{2+}, Mg^{2+}, Mn^{2+}, Sr^{2+}, K^+, Ba^{2+}, Cd^{2+}, Al^{3+}, and Co^{2+}) was studied in DMSO. As depicted in Fig. 2A, compound **1o** alone showed no significant emission signal at 520 nm excitation, however, the **1o**'s solution exhibited strong fluorescence with an approximate 34-fold enhancement in the fluorescence intensity at 617 nm upon the addition of 10.0 equiv. of Hg^{2+}. Though the **1o** also responded to Cr^{3+} and Fe^{3+}, the fluorescence emission intensity

only enhanced 10-fold and 6-fold at 617 nm, respectively. Other metal ions didn't cause detectable increase in the emission intensity (Fig. 2C). The result indicated that the **1o** had a relatively higher binding affinity to Hg^{2+} than Cr^{3+} or Fe^{3+}, and **1o** can be potentially used as a chemosensor for detecting Hg^{2+} in DMSO. Further, the competitive experiments were conducted by adding Hg^{2+} to DMSO-solution of **1o** in the presence of other metal ions. As a result, the Hg^{2+} induced spectral enhancement was not affected by the tested background metal ions (Fig. 2B).

The fluorescence titration experiments were performed to survey sensitive property of **1o** to Hg^{2+}. As shown in Fig. 3A and B, free **1o** displayed no fluorescent emission at 617 nm upon excitation at 520 nm. With increasing amounts of Hg^{2+} (0–10.0 equiv.), the fluorescent intensity gradually increased about 34-fold at 617 nm, accompanied with a fluorescence change of color from dark to orange-red. The absolute fluorescent quantum yield of **1o**-Hg^{2+} (**1o′**) was measured to be 0.35. The spectral fitting of the fluorescence data obtained by titration experiments of **1o** with Hg^{2+} shows the formation of 1 : 1 stoichiometric **1o**-Hg^{2+} complex with a binding constant 0.42×10^4 M^{-1} (Fig. S4†).[37] The detection limit of Hg^{2+} was determined to be 0.14 μM (Fig. S5†).[38] Hence, **1o** could be used as a fluorescence chemosensor to detect Hg^{2+} with high sensitivity.

The fluorescent intensity and color of **1o**-Hg^{2+} could restore the initial state by the addition of EDTA (10.0 equiv.), attesting the reversibility for the coordination of **1o** with Hg^{2+}. Also noteworthy is that complex **1o**-Hg^{2+} showed excellent
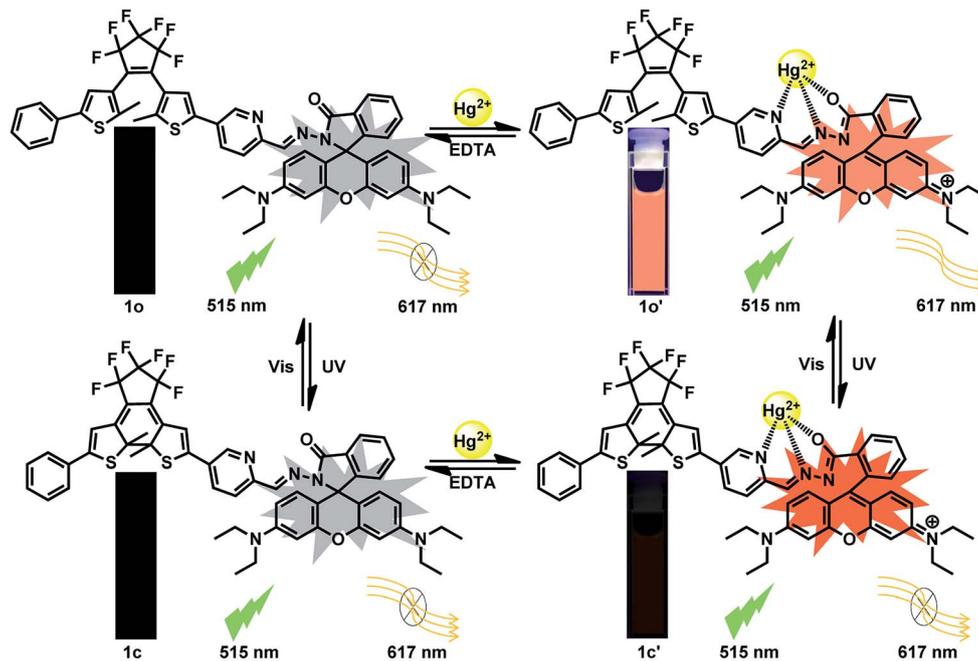
Scheme 3 Dual-controlled fluorescent switching behavior of **1o** induced by the stimulation of Hg^{2+}/EDTA and UV/vis light.

photoswitching properties under alternate UV/vis irradiation. Upon irradiation with 297 nm UV light, the fluorescence emission intensity of **1o**-Hg^{2+} complex was quenched 73.6% due to the formation of the weak fluorescent isomer **1c**-Hg^{2+} (**1c′**) (Fig. S6†). Upon being illuminated with visible light, the fluorescent intensity of **1o**-Hg^{2+} could be restored. Based on these features, a dual-responsive and reversible fluorescent molecular switch could be constructed (Scheme 3).

To further investigate the stoichiometry of the **1o**-Hg^{2+} complex, Job's plot experiment for fluorescence measurement was performed (Fig. 4A). The fluorescence reached a maximum value when the ratio of $[1o]/[(1o) + (Hg^{2+})]$ was 0.5, indicating a 1 : 1 binding stoichiometry between Hg^{2+} and **1o** in the complex. Subsequently, the ESI-MS analyses were performed to further verify the complexation stoichiometry of **1o** and Hg^{2+} (Fig. 4B). A new peak at $m/z = 1251.9$ corresponding to [**1o** +

$Hg^{2+} + NO^{3-}]^+$ was observed after the addition of Hg^{2+} to the solution of **1o**. This result also supported that **1o** and Hg^{2+} formed a 1 : 1 complex. ^1H NMR titration experiments were employed to gain a deep understanding on the coordination between **1o** and Hg^{2+} (Fig. S7†). Upon the addition of Hg^{2+}, the proton peaks at 8.82, 8.14, 8.01 ppm for pyridine (Ha, Hc and Hd) and 8.28 ppm for CH=N (Hb) broadened and downfield shifted, owing to the decreasing of electron density after coordination with Hg^{2+}.[39] Herein, combined with our previous knowledge,[40,41] we proposed a possible binding mode of Hg^{2+} with **1o** (Fig. S7†).

Colorimetric responses of 1o toward Cu^{2+}

The colorimetric responses of **1o** (20 μM) to different metal ions including Cu^{2+}, Hg^{2+}, Cr^{3+}, Al^{3+}, Fe^{3+}, Cd^{2+}, Ba^{2+}, K^+, Ni^{2+}, Sr^{2+},
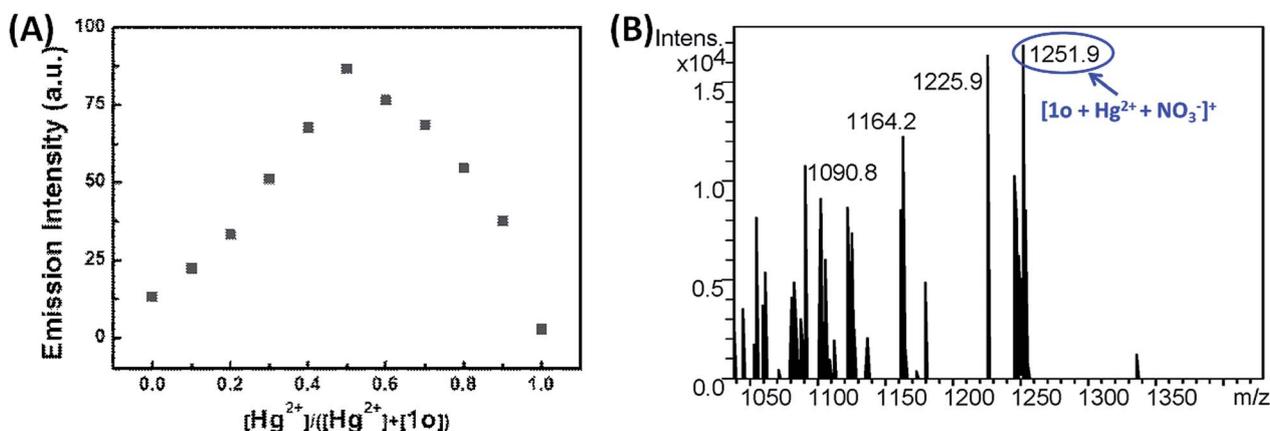

Fig. 4 (A) Job's plot for determining the stoichiometry of **1o** and Hg^{2+}. (B) ESI-MS spectrum of **1o′**.
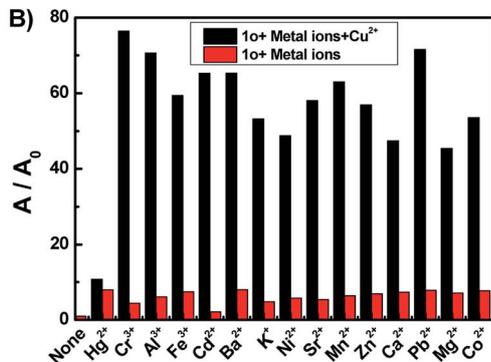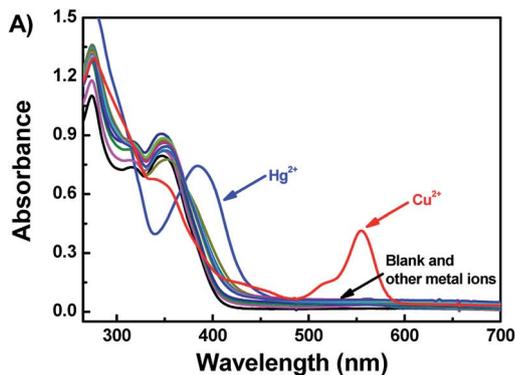
Fig. 5 (A) Absorption spectra of **1o** (20 μM) in the presence of various metal ions (10.0 equiv.) in THF. (B) Effect of competitive metal ions on the interaction between **1o** and Cu^{2+} ion. (C) The color of **1o** upon addition of various metal ions.

Fig. 6 (A) Absorption spectra changes of **1o** in THF induced by Cu^{2+}/EDTA. (B) Absorption at 555 nm versus equivalents of Cu^{2+} added.

Scheme 4 The binding mode between **1o** and Cu^{2+}.

Mn^{2+}, Zn^{2+}, Ca^{2+}, Pb^{2+}, Mg^{2+}, and Co^{2+} were investigated in THF. The free **1o** showed no absorption in the spectral range 500–600 nm, suggesting that the rhodamine moiety adopts a closed spirolactam form. As shown in Fig. 5A, with the addition of 10.0 equiv. of each kind of ions, only Cu^{2+} could induce a prominent change (a strong absorption at 555 nm). The color of **1o** solution changed from colorless to pink upon the addition of Cu^{2+}, which indicated the formation of **1o**-Cu^{2+} (**1o″**) with rhodamine moiety in ring-opened form (Fig. 5C).[42] A series of competitive tests of the background metal ions were also carried out (Fig. 5B). The absorbance at 555 nm decreases almost to the initial state when the same amount of Hg^{2+} was added. The result revealed that Cu^{2+} detection by **1o** was little affected by the presence of other metal ions except for Hg^{2+}.

To further investigate the sensing mechanism of **1o** with Cu^{2+} ion, UV-vis absorption titration experiments were performed. Upon gradual addition of Cu^{2+} (0–10.0 equiv.), the absorption band centered at 555 nm gradually enhanced and reached a plateau when 10.0 equiv. of Cu^{2+} was added (Fig. 6A). The color of the **1o** solution changes from colorless to pink, due
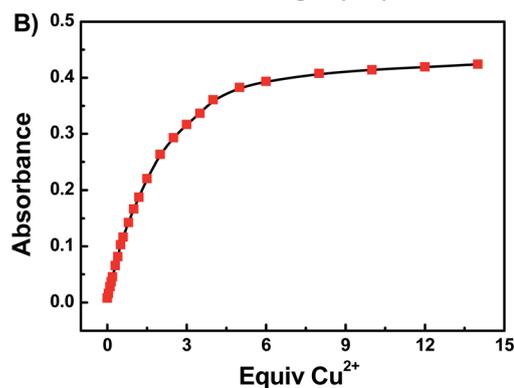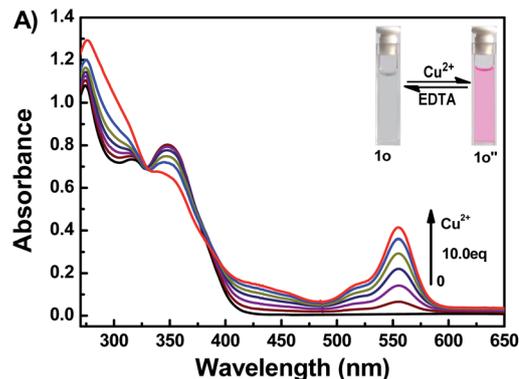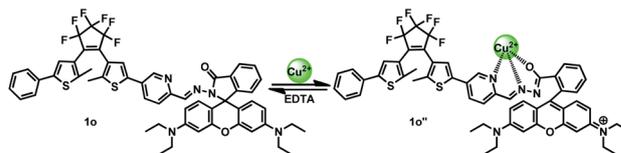
to the formation of the **1o**-Cu^{2+} (**1o″**) complex. There was an isosbestic points at 329 nm demonstrate that the complexation reaction between Cu^{2+} and **1o** exist in equilibrium.[43] Furthermore, the absorbance and the solution color could be reverted to the initial state upon the addition of excess of EDTA. From the absorption titration experiments, the absorbances of **1o** at 555 nm were plotted as a function of the Cu^{2+} concentration (Fig. 6B). Within the range of 0–30 μM, a linear relationship ($Y = 0.00723X + 0.01803$, $R = 0.992$) can be observed (Fig. S8†). The binding constant of **1o** to Cu^{2+} was found to be 1.76×10^4 M^{-1} ($R = 0.999$) (Fig. S9†). The detection limit for Cu^{2+} was estimated to be 0.51 μM (Fig. S10†).

To further ascertain the mechanism, Job's plot, ESI-MS and ^1H NMR titration experiment were performed. The absorption intensity at 555 nm reached the maximum value when the molar fraction of Cu^{2+} and **1o** was 0.5, which indicated that **1o** bounded to Cu^{2+} with a 1 : 1 stoichiometry (Fig. S11†). Further evidence for the 1 : 1 binding stoichiometry between Cu^{2+} and **1o** was obtained by ESI-MS (Fig. S12†). Upon the addition of
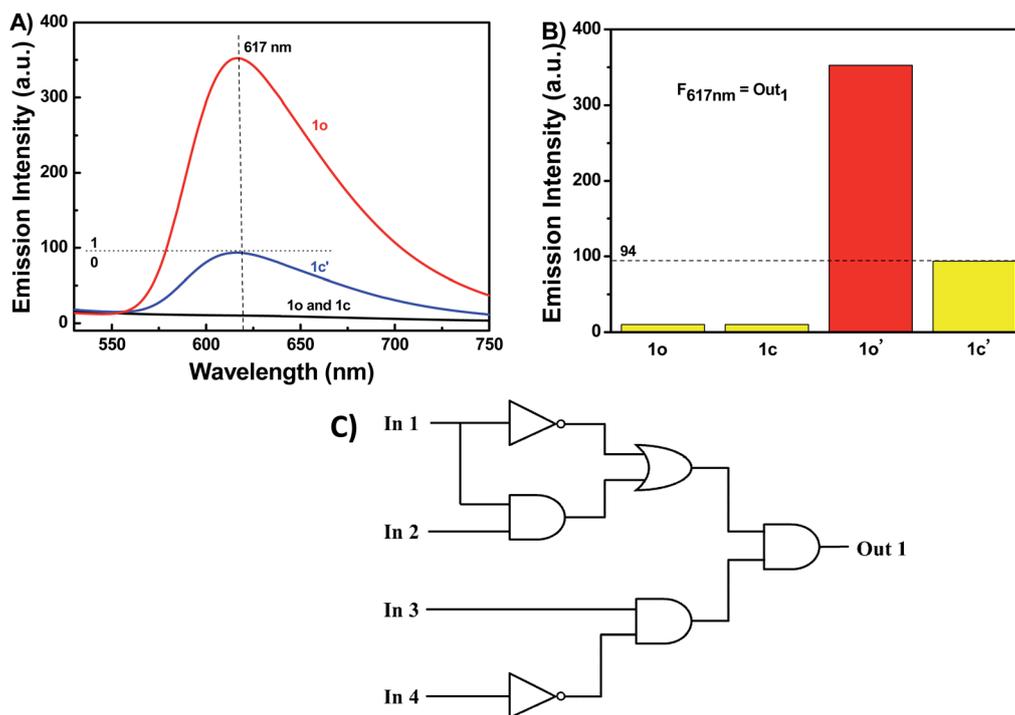
Fig. 7 (A) Fluorescence spectra of **1o** in the presence of Hg^{2+} (10 equiv.) and UV light (the dotted line represent the threshold value). (B) Histogram of fluorescence intensities at 617 nm. (C) The logic diagram.

Cu^{2+}, a new peak at $m/z = 1112.0$ corresponding to $[1o + Cu^{2+} + NO^{3-}]^+$ was observed, which also confirmed the 1 : 1 stoichiometric ratio of $Cu^{2+}/1o$. To better understand the interaction between **1o** and Cu^{2+}, ^1H NMR titration experiments were performed (Fig. S13†). With the addition of Cu^{2+}, the proton peaks at 9.03, 7.81, 7.71 ppm for pyridine (Ha, Hc and Hd) and
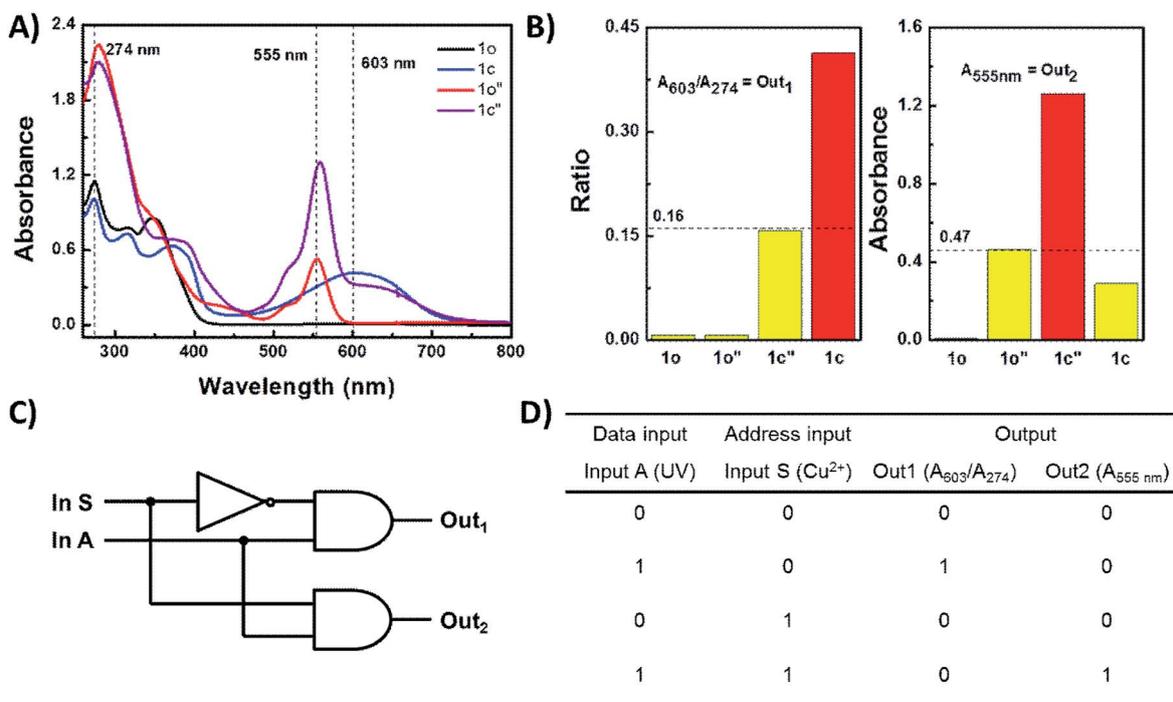

Fig. 8 (A) Absorption spectra changes of **1o** in the presence of Cu^{2+} (10 equiv.) and UV light (the dotted lines represent the thresholds separating output signals). (B) Histogram of the absorbance ratio of (A_{603}/A_{274}) and the absorbance at 555 nm. (C) The logic diagram. (D) The truth table for the 1 : 2 demultiplexer.

8.59 ppm for CH=N (Hb) broadened and downfield shifted, owing to the decreasing of electron density after coordination with Cu^{2+}.[39] Similar observations have been reported for other ion probes.[44] Based on these results, together with previous reports, a bonding mode has been proposed as shown in Scheme 4.

Applications in logic circuit

Moreover, a molecular logic circuit was constructed with four inputs and one output based on the fluorescence behavior induced by lights and chemical stimuli (Fig. 7A and C). The four input signals were In 1: 297 nm UV light, In 2: visible light ($\lambda <$ 500 nm), In 3: Hg^{2+}, and In 4: EDTA, while the fluorescence intensity of **1o** at 617 nm was used as the output signal (fluorescence intensity ≤ 94 was assigned the boolean value "0" and fluorescence intensity > 94 was assigned the logical value "1") (Fig. 7B). For instance, if the input string is '0, 1, 1, and 0', corresponding to In 1, In 2, In 3, and In 4 in the 'off, off, on, and off' state. Under these conditions, the emission intensity was enhanced notably due to the formation of **1o**-Hg^{2+} complex, resulting in an output state of 'on' with a digit of '1'. The truth table of the combinational circuit was presented in Fig. S14.†

Owing to significant absorption changes of **1o** stimulated by ultraviolet and Cu^{2+} it would be able to act as a 1 : 2 digital demultiplexer (Fig. 8A). The data input (In A) was UV light, the address input (In S) was Cu^{2+}, the two outputs were the absorbance at 555 nm and the absorbance ratio of (A_{603}/A_{274}), respectively. Fig. 8D shows the absorbance output levels measured for a solution of **1o** in THF under the conditions corresponding to the four possible combinations of inputs. After determining a suitable threshold for the absorbance output, the truth table for the operation of the **1o**-based digital multiplexer was obtained (Fig. 8B). The binary data and address inputs can exist in one of two states, on (1) or off (0). The outputs, Out 1 and Out 2 may likewise be set either on (1) or off (0). When In S (or address input) is set off then Out 1 (A_{603}/A_{274}) reports the state of In 1 (UV) and Out ($A_{555\ nm}$) remains off, conversely, when In S is switched on, Out 2 replaces Out 1 to report the state of In A and Out 1 turns off. The corresponding logic circuit was shown in Fig. 8C.

Conclusions

In summary, a novel chemosensor based on a diarylethene containing a rhodamine B unit was developed. It can act as a selective fluorescence chemosensor for Hg^{2+} in DMSO, with a detection limit of 0.14 μM. It is also a naked-eye probe for Cu^{2+} in THF, with a detection limit of 0.51 μM. Furthermore, the fluorescence of the **1o**-Hg^{2+} complex was efficiently adjusted by alternating UV/vis lights. A 1 : 2 demultiplexer circuit was constructed by using UV light as data input, Cu^{2+} as the address input, and the absorbance at 555 nm and the absorbance ratio of (A_{603}/A_{274}) as the dual data outputs. This work may contribute to the design and construct of other diarylethene based multifunctional chemosensors.

Conflicts of interest

There are no conflicts of interest to declare.

Acknowledgements

Notes and references

1 J. F. Zhang, Y. Zhou, J. Yoon and J. S. Kim, *Chem. Soc. Rev.*, 2011, **40**, 3416–3429.
2 A. P. de Silva, H. Q. Gunaratne, T. Gunnlaugsson, A. J. Huxley, C. P. McCoy, J. T. Rademacher and T. E. Rice, *Chem. Rev.*, 1997, **97**, 1515–1566.
3 P. B. Tchounwou, W. K. Ayensu, N. Ninashvili and D. Sutton, *Environ. Toxicol.*, 2003, **18**, 149–175.
4 H. N. Kim, W. X. Ren, J. S. Kim and J. Yoon, *Chem. Soc. Rev.*, 2012, **41**, 3210–3244.
5 W. F. Fitzgerald, C. H. Lamborg and C. R. Hammerschmidt, *Chem. Rev.*, 2007, **107**, 641–662.
6 G. Guzzi and C. A. La Porta, *Toxicology*, 2008, **244**, 1–12.
7 J. C. Clifton 2nd, *Pediatr. Clin. North Am.*, 2007, **54**, 237–269.
8 E. Gaggelli, H. Kozlowski, D. Valensin and G. Valensin, *Chem. Rev.*, 2006, **106**, 1995–2044.
9 D. J. Waggoner, T. B. Bartnikas and J. D. Gitlin, *Neurobiol. Dis.*, 1999, **6**, 221–230.
10 T. R. Halfdanarson, N. Kumar, C. Y. Li, R. L. Phyliky and W. J. Hogan, *Eur. J. Haematol.*, 2008, **80**, 523–531.
11 S. R. Jaiser and G. P. Winston, *J. Neurol.*, 2010, **257**, 869–881.
12 D. Pramanik, C. Ghosh and S. G. Dey, *J. Am. Chem. Soc.*, 2011, **133**, 15545–15552.
13 J. C. Lee, H. B. Gray and J. R. Winkler, *J. Am. Chem. Soc.*, 2008, **130**, 6898–6899.
14 E. Tiffany-Castiglioni, S. Hong and Y. Qian, *Int. J. Dev. Neurosci.*, 2011, **29**, 811–818.
15 E. V. Stelmashook, N. K. Isaev, E. E. Genrikhs, G. A. Amelkina, L. G. Khaspekov, V. G. Skrebitsky and S. N. Illarioshkin, *Biochemistry*, 2014, **79**, 391–396.
16 M. Irie, T. Fukaminato, K. Matsuda and S. Kobatake, *Chem. Rev.*, 2014, **114**, 12174–12277.
17 J. J. Zhang and H. Tian, *Adv. Opt. Mater.*, 2018, **6**, 1701278.
18 J. F. Lv, G. Liu, C. B. Fan and S. Z. Pu, *Spectrochim. Acta, Part A*, 2020, **227**, 117581.
19 S. van de Linde and M. Sauer, *Chem. Soc. Rev.*, 2014, **43**, 1076–1087.
20 S. Z. Pu, C. H. Zheng, Q. Sun, G. Liu and C. B. Fan, *Chem. Commun.*, 2013, **49**, 8036–8038.
21 M. Takeshita, E. Mizukami, K. Murakami, Y. Wada and Y. Matsuda, *Eur. J. Org. Chem.*, 2014, 3784–3787.
22 J. F. Lv, Y. L. Fu, G. Liu, C. B. Fan and S. Z. Pu, *RSC Adv.*, 2019, **9**, 10395–10404.

23 L. Xu, S. Wang, Y. N. Lv, Y. A. Son and D. R. Cao, *Spectrochim. Acta, Part A*, 2014, **128**, 567–574.

24 Y. F. Liang, R. J. Wang, G. Liu and S. Z. Pu, *ACS Omega*, 2019, **4**, 6597–6606.

25 Y. L. Fu, C. B. Fan, G. Liu, S. Q. Cui and S. Z. Pu, *Dyes Pigm.*, 2016, **126**, 121–130.

26 G. Li, F. R. Tao, H. Wang, L. P. Wang, J. J. Zhang, P. P. Ge, L. Liu, Y. H. Tong and S. Sun, *RSC Adv.*, 2015, **5**, 18983–18989.

27 G. Li, L. P. Bai, F. R. Tao, A. X. Deng and L. P. Wang, *Analyst*, 2018, **143**, 5395–5403.

28 S. Z. Pu, H. C. Ding, G. Liu, C. H. Zheng and H. Y. Xu, *J. Phys. Chem. C*, 2014, **118**, 7010–7017.

29 H. M. Kang, C. B. Fan, H. T. Xu, G. Liu and S. Z. Pu, *Tetrahedron*, 2018, **74**, 4390–4399.

30 H. T. Xu, H. C. Ding, G. Li, C. B. Fan, G. Liu and S. Z. Pu, *RSC Adv.*, 2017, **7**, 29827–29834.

31 W. J. Liu, S. Z. Pu, D. H. Jiang, S. Q. Cui, G. Liu and C. B. Fan, *Microchim. Acta*, 2011, **174**, 329–336.

32 D. B. Zhang, S. Y. Li, R. M. Lu, G. Liu and S. Z. Pu, *Dyes Pigm.*, 2017, **146**, 305–315.

33 J. L. Li, G. H. Ding, Y. Y. Niu, L. Y. Wu, H. J. Feng and W. Y. He, *Spectrochim. Acta, Part A*, 2018, **200**, 127–135.

34 H. M. Kang, C. B. Fan, G. Liu and S. Z. Pu, *Spectrochim. Acta, Part A*, 2019, **211**, 322–329.

35 Z. Wang, S. Q. Cui, S. Y. Qiu and S. Z. Pu, *Tetrahedron*, 2018, **74**, 7431–7437.

36 S. Q. Cui, S. Y. Qiu, R. M. Lu and S. Z. Pu, *Tetrahedron Lett.*, 2018, **59**, 3365–3372.

37 H. Ye, F. Ge, X. C. Chen, Y. Li, H. Zhang, B. X. Zhao and J. Y. Miao, *Sens. Actuators, B*, 2013, **182**, 273–279.

38 Y. F. Liang, L. Diao, R. J. Wang, N. S. Wang and S. Z. Pu, *Tetrahedron Lett.*, 2019, **60**, 106–112.

39 G. Zhao, F. F. Song, G. Wei, R. L. Wu, Z. Yan, F. Y. Zhang, S. Y. Guang and H. Y. Xu, *Sens. Actuators, B*, 2019, **286**, 163–172.

40 D. Y. Wu, W. Huang, C. Y. Duan, Z. H. Lin and Q. J. Meng, *Inorg. Chem.*, 2007, **46**, 1538–1540.

41 P. Sakthivel, K. Sekar, G. Sivaraman and S. Singaravadivel, *New J. Chem.*, 2018, **42**, 11665–11672.

42 H. Seo, M. E. Jun, K. Ranganathan, K. H. Lee, K. T. Kim, W. Lim, Y. M. Rhee and K. H. Ahn, *Org. Lett.*, 2014, **16**, 1374–1377.

43 Y. Wang, H. Wu, W. N. Wu, X. J. Mao, X. L. Zhao, Z. Q. Xu, Z. H. Xu and Y. C. Fan, *Spectrochim. Acta, Part A*, 2019, **212**, 1–9.

44 Y. Zhang, X. Zeng, L. Mu, Y. Chen, J. X. Zhang, C. Redshaw and G. Wei, *Sens. Actuators, B*, 2014, **204**, 24–30.